

## Autonomous wireless radar sensor mote for target material classification



Muhammad M.R. Khan<sup>a</sup>, Khan M. Iftexharuddin<sup>b,\*</sup>, Ernest McCracken<sup>c</sup>,  
Khandakar Islam<sup>a</sup>, Sushil Bhurtel<sup>a</sup>, Lan Wang<sup>c</sup>, Robert Kozma<sup>d</sup>

<sup>a</sup> Department of Electrical & Computer Engineering, University of Memphis, Memphis, TN, United States

<sup>b</sup> Department of Electrical & Computer Engineering, Old Dominion University, Norfolk, VA, United States

<sup>c</sup> Department of Computer Science, University of Memphis, Memphis, TN, United States

<sup>d</sup> Department of Mathematical Sciences, University of Memphis, Memphis, TN, United States

### ARTICLE INFO

#### Article history:

Available online 5 December 2012

#### Keywords:

Wireless sensor network  
Doppler radar  
Radar signal processing  
Radar cross section  
Mathematical model of reflectivity  
Target classification

### ABSTRACT

Autonomous wireless sensor networks consisting of different types of sensor modalities have been receiving greater attention from researchers due to their versatility and portability. These autonomous sensor networks commonly include passive sensors such as infrared, acoustic, vibration, and magnetic nodes. However, fusion of active sensors in the integrated sensor network, such as Doppler radars, may offer powerful capabilities for many different sensing and classification tasks. In this work, we demonstrate the design and implementation of an autonomous wireless sensor network integrating a Doppler sensor with commercial off-the-shelf components. We investigate the effect of various types of target materials on the measured radar signal as one of the applications of the newly designed radar–mote network. Different types of materials affect the amount of energy reflected back to the source of an electromagnetic wave. We obtain mathematical and simulation models for the reflectivity of different homogeneous non-conducting materials and study the effect of such reflectivity on the classification of targets. We validate our simulation results using real experimental data collected through our autonomous radar–mote sensor network using various types of targets.

© 2012 Elsevier Inc. All rights reserved.

### 1. Introduction

Autonomous wireless sensor networks with different sensor modalities are the objective of active research due to the versatility and portability of their applications [1–5]. An autonomous sensor network is a collection of sensor nodes with limited processing, power, and communication capabilities that monitors a real world environment with limited or no human intervention. In a typical monitoring application, each node of the network gathers information about the local environment, preprocesses the data, and transmits via wireless channels to a base station [1,3]. Historically, this type of autonomous systems typically used infrared, acoustic, vibration, and magnetic sensors for passive sensing, and optic and ultrasound sensors for active sensing. However, Radio Detection And Ranging (Radar) has not been used extensively in wireless sensor networks except in a few research studies (e.g., [2]). Radar systems are widely used in defense, meteorology and surveillance due to their versatility in working from a long range, in adverse weather where other sensors may be unavailable, or with non-cooperative targets. Radar is an object detection system

that uses electromagnetic waves to identify the range, altitude, direction, and speed of moving and fixed objects such as aircraft, ships, motor vehicles, clouds, storms and terrain [6]. In addition to the precise range and velocity measurements of the target objects, radar systems have the capability to classify targets based on the Radar Cross Section (RCS) of different objects. Such classification capability is related to the electromagnetic energy reflected back from various classes of objects. The types of materials affect the amount of reflection from an object [7,8]. The application of Doppler radar has been limited in wireless sensor networks because conventional systems are expensive, bulky, and difficult to use with very few exceptions [2]. Currently, with the advancement of technology, a large variety of small, inexpensive radar sensors with standard capabilities and low power requirements are commercially available [9]. Therefore, there is an opportunity to integrate a radar sensor with autonomous distributed wireless sensors.

The integration of radar into autonomous sensor systems provides a powerful and robust sensing modality that complements the already available modalities, such as acoustic, magnetic, vibration, and passive infrared sensors. Effective integration designs can provide a powerful distributed sensor network system with versatile sensor modalities. In the integrated system, radar offers measurements of the range, velocity, direction, and electromagnetic

\* Corresponding author.

E-mail address: kiftekh@odu.edu (K.M. Iftexharuddin).

characteristics of the target to complement existing wireless sensor node capabilities [10,11]. The intelligent combination of some or all of the sensor modalities in certain application scenarios can work as an effective tool to detect, track, and identify targets in wide areas. The successful design and implementation of integrated autonomous distributed sensor network may provide a low tier data gathering system to be used with an intelligent decision support system [10,11]. Furthermore, the successful development of the integrated sensor system using the commercially available low-cost products would be useful for widespread civil and defense applications.

In this work, we design and implement an autonomous distributed sensor network that integrates a low-cost tiny Doppler radar sensor with the commercially available wireless sensor motes for dynamic surveillance and tracking. Our autonomous distributed sensor network is then used to collect data from an indoor experimental setup. The data collected from the network is stored and analyzed in a computer system connected to a base station. We investigate the effect of different types of materials using Doppler radars in the integrated sensor system. The material property is an important factor that influences how much electromagnetic energy is reflected back to the source from where it emits. For simplification of the model and the limited scope of this work, we investigate the reflectivity of the non-conducting materials only. The relation between refractive index of non-conducting materials and the reflectivity of plain electromagnetic wave from non-conducting materials can be modeled mathematically [7,8]. We modify the reflectivity model to incorporate the Doppler principle and simulate the effects of Doppler signals reflected from non-conducting materials. Then radar reflection data from non-conducting material surfaces is collected using our integrated radar–mote autonomous system. Finally, we classify different types of non-conducting materials based on the radar signals reflected back from the corresponding material surfaces. In summary, the objectives of this work are as follows:

- i. Design and implement a wireless autonomous radar–mote sensor network integrating a Doppler radar into a wireless sensor node with low-cost commercial off-the-shelf components.
- ii. Investigate the effect of different types of target materials on return radar signal and use the newly built integrated radar–mote sensor network as data collection tool for the investigation.

The paper is organized in multiple sections. In Section 2, we review relevant background research and the essential technologies required for this work. In Section 3, we first briefly describe the proposed design and implementation of an integrated radar–mote autonomous system. We then present the modified reflectivity model to show how material property affects the reflection of electromagnetic waves. In addition, we present a simple signal processing algorithm to classify different types of materials. In Section 4, we first describe our data collection process using our integrated experimental setup. We then compare simulated and experimental reflectivity of non-conducting materials. Moreover, we present the classification of different types of non-conducting materials using our electromagnetic reflection model. We also discuss the advantages of our system compared with standalone radar systems and other mote systems. Finally, we discuss our conclusion and future work in Section 5.

## 2. Background review

In this section, we briefly review relevant recent research efforts and background materials describing the integration of radar

sensors with wireless motes and various applications. The capability of these sensor networks is also discussed from a theoretical point of view. Finally, we describe the theoretical model showing the relation between material refractive index and reflectivity of electromagnetic signal [7,8].

### 2.1. Previous research efforts on integrated radar–mote sensor networks and their applications

Radar has been conspicuously absent from integrated sensor systems because radar systems are typically quite bulky. With the advent of the micro-power pulse radar at Lawrence Livermore National Labs in mid 1990s, low power radars became a possibility. Subsequently, technical progress in sensor networks has led the effort to integrate radar as one of the sensor modalities to sensor network platform.

The radar–mote, designed by researchers at UC Berkeley and Ohio State University, consists of several circuit boards including a main processor and radio board, an optional sensor board, an ultra wideband radar sensor, and a power board [2]. They use Mica2 sensor mote and 2.4 GHz TWR-ISM-002 radar sensor from Advantaca [12] as two main components of their radar-enabled sensor network. BumbleBee is an integrated radar–mote sensor developed by the Samraksh Company [13] that includes a low-power Pulsed Doppler Radar (PDR). The key features of the BumbleBee include: a detection range between 1 m to 10 m that is controllable via software, coherent output (both  $I$  and  $Q$  channels), on-board internal antenna, 60 degree conical coverage pattern, and detection of radial velocities between 2.6 cm/s and 2.6 m/s [13]. The BumbleBee package includes a BumbleBee radar board and a TelosB or TMote Sky mote. The BumbleBee is suitable for variety of monitor and surveillance applications [13].

Although these integrated radar–mote sensor network products work well for certain applications, there is still room for improvement. According to the BumbleBee's user manual [13], complex signal post-processing is required to compute range information using BumbleBee. Furthermore, since BumbleBee is not intended to be used as a ranging radar, it does not produce range information simultaneously with velocity in general [13]. It is of great practical benefit to have a radar–mote system with high sampling rate, which computes the range and velocity simultaneously with simple signal processing techniques. Our system accomplishes this goal.

### 2.2. Components of our autonomous sensor network

Our integrated system includes a TelosB wireless mote from Crossbow Technology [14] and a  $K_a$ -band Doppler transceiver from M/A-Com Tech [15]. We integrate a  $K_a$ -band Doppler Radar into the wireless node so that it can detect range and velocity of target object simultaneously. We use a horn antenna with the Doppler radar that sends a signal more specific to a target direction.

#### 2.2.1. TelosB mote platform details

Crossbow's TelosB mote (TPR2400) is an open source platform designed for the research community [14]. The TPR2400 includes the standard features such as USB programming capability, an IEEE 802.15.4 standard radio transceiver with built-in antenna, a low power microcontroller (MSP430), and capability to integrate sensor boards through standard ports. Fig. 1 shows a picture of TelosB mote and its block diagram.

#### 2.2.2. $K_a$ -band Doppler transceiver (MACS-007802-0M1R1V)

We select a  $K_a$ -band (24–40 GHz) Doppler transceiver from M/A-Com Tech for our integrated radar–mote sensor suite. It is a low-cost (\$50) and low-power Doppler transceiver that suits

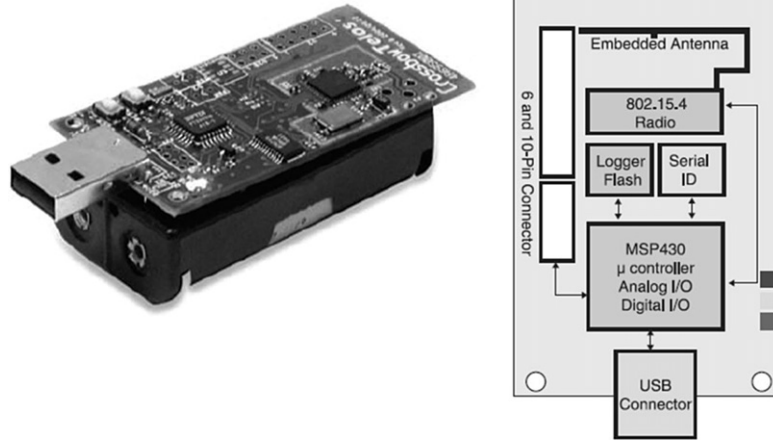


Fig. 1. (a) TelosB TPR2400 mote real picture (left), (b) block diagram of TelosB TPR2400 mote (right) (source: Ref. [14]).

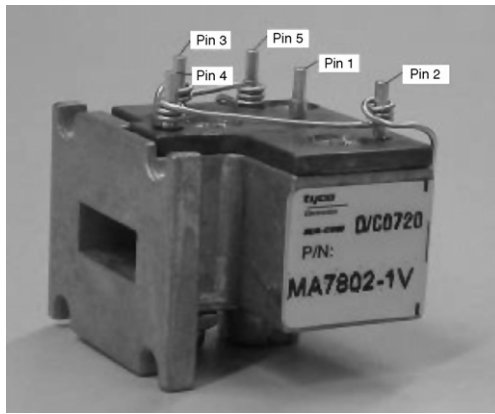


Fig. 2. Doppler transceiver (MACS-007802 0M1RSV) (source: Ref. [15]).

Table 1

Pin configuration of the Doppler transceiver (MACS-007802-0M1RSV).

| PIN | Function           |
|-----|--------------------|
| 1   | DC input           |
| 2   | Ground             |
| 3   | IF output (Mixer1) |
| 4   | IF output (Mixer2) |
| 5   | Vtune input        |

our goal. This M/A-COM RF transceiver (Model MACS-007802-0M1RSV) is primarily used for automotive applications such as front and rear-ends collision detection, in-ground speed measurement, and as motion detectors in automatic door systems [15]. The transceiver is very small in size ( $< 1$  inch on each side), resembling an ice cube, which makes it an excellent choice for our autonomous integrated radar-mote sensor network system. The radar transmits a continuous wave at 24.125 GHz and it has an electronic tuning system that varies the frequency within a bandwidth of 0.3 GHz. An external voltage ramp pulse can be applied to the electronic or voltage tune input of the radar causing the radar to emit continuous frequency-modulated signal of 300 MHz bandwidth. The signal received by the radar through antenna is mixed with the transmitted wave and low-pass filtered to produce In-phase ( $I$ ) and Quadrature ( $Q$ ) output which are available on pin 3 and 4 of the radar respectively. Fig. 2 and Table 1 show the Doppler transceiver and the organization of its pins.

### 2.3. Radar signal processing of range and range-rate data

By applying different voltages to the electronic tuning input of the Doppler radar, we can vary the frequency from a minimum value  $f_0$  to a maximum value  $f_1$  between 24 to 24.3 GHz. In this section, we discuss how we can use this frequency variation to measure target range and velocity. To cover the frequency band quickly we use ramp voltages as voltage tune input, which generates a continuous sweep from low to high frequency. When an object moves away from the radar, it causes the reflected signal to down shift slightly relative to the transmitted signal. The reverse occurs when the object moves toward the radar. The radar receiver mixes the transmitted and shifted received signal and passes it through the low-pass filter. The final radar output oscillates at the Doppler frequency, which is proportional to the range-rate or velocity of the target object. We can get the magnitude of range-rate by capturing any of the output channel signal of the radar and then computing the Fast Fourier Transform (FFT) [16,17]. Moreover, we can get the direction of the moving target in addition to range-rate by processing the two output channels together.

Consider that the Doppler radar transceiver emits a continuous frequency sinusoidal signal as follows [16,17],

$$x_0(t) = \cos(2\pi f_0 t + \Phi), \quad (1)$$

here,  $f_0$  is the carrier frequency,  $t$  is time and  $\Phi$  is some random phase. The transmitted signal is then propagated to a stationary target, reflected, and propagated back to the Doppler transceiver. The received signal is the replica of the transmitted signal with a propagation delay corresponding to the round trip time required for the propagation of the signal. If we assume that the transmitter and receiver are synchronized with same clock, this propagation delay can be represented as  $= 2r/c$ , where  $r$  is the distance between the radar and the target object in meter and  $c = 3 \times 10^8$  m/s is the propagation velocity of the microwave signal. Now the received signal can be expressed as:

$$\begin{aligned} x_r(t) &= \sigma x_0(t - \Delta t) = \sigma x_0(t - 2r/c) \\ &= \sigma \cos[2\pi f_0 t + \Phi - 4\pi f_0 r/c], \end{aligned} \quad (2)$$

where  $\sigma$  is a constant that corresponds to the target radar cross section (RCS), geometric attenuation of the signal as well as other terms related to the target object and signal characteristics. At the receiver end of the Doppler transceiver circuitry, the received and transmitted signals are multiplied and then filtered using low-pass filter. The filtered signal output from the mixer is simplified using the trigonometric identity,  $2 \cos a \cdot \cos b = \cos(a + b) + \cos(a - b)$ , and we get the mixer output expressed as follows,

$$F_{mix}(t) = \frac{\sigma}{2} \cos[4\pi f_0 t + 2\Phi - 4\pi f_0 r/c] + \frac{\sigma}{2} \cos[4\pi f_0 r/c]. \quad (3)$$

This mixer output signal is the summation of two terms having frequency  $2f_0$  and a constant DC bias. If the sinusoidal signal is discarded using a low-pass filter, we get the following signal as the radar output which is a function of the target range  $r$ :

$$I = \frac{\sigma}{2} \cos[4\pi f_0 r/c]. \quad (4)$$

Now based on the relation between propagation delay  $\Delta t$  and  $r$ , the range-rate or velocity expressions are derived. If the target object is changing the range at a constant rate  $\dot{r}$  meters/s then,

$$r(t) = r_0 + \dot{r}t, \quad (5)$$

where  $r_0$  is range at time instant zero. Putting the value of  $r$  into Eq. (2) and rearranging the term we get,

$$x_r(t) = \sigma \cos\left[2\pi(f_0 + \Delta f)t - \frac{4\pi f_0 r_0}{c} + \Phi\right], \quad (6)$$

where  $\Delta f = -(2\dot{r}/c)f_0$  and  $\Delta f$  is known as Doppler frequency shift [16]. From Eq. (4), it is evident that the reflected signal downshifts slightly relative to the transmitted signal when an object moves away from the radar. The radar receiver mixes the transmitted and shifted received signal and passes it through the low-pass filter. The low-pass filtered signal after simplification with cosine identity can be expressed as,

$$I(t) = \frac{\sigma}{2} \cos\left[2\pi(\Delta f)t - \frac{4\pi f_0 r_0}{c}\right]. \quad (7)$$

The final radar output oscillates at Doppler frequency  $\Delta f$ . From the relation between  $\Delta f$  and  $\dot{r}$  we see that Doppler frequency is proportional to range-rate or velocity of the target object. We can get the magnitude of range-rate  $\dot{r}$  by capturing the  $I(t)$  signal with a storage oscilloscope and then computing the Fast Fourier Transform (FFT).

By using the  $I$ -component of the Doppler data, it is possible to estimate the target velocity by sampling the outputs with an oscilloscope and applying FFT. However, if we use the  $I$ -channel data only, we cannot determine the direction of movement without ambiguity. By using the Quadrature component ( $Q$ ) of dual channel radar we can combine  $I$  and  $Q$  into a complex signal,  $F(t) = I(t) + iQ(t)$ , where  $Q$ -channel data is the 90 degree phase shifted version of the  $I$ -channel data. Now application of FFT to the complex signal allows us to get rid of the twin peaks. In our experiment we capture  $I$ -channel and assign zero to the  $Q$ -channel. In the rest of this section we briefly describe how to use ramp pulses for computing range and velocity based on the above discussion.

The Doppler radar that we use has an electronic tuning input with frequency band 24 to 24.3 GHz. To cover the frequency band quickly we use ramp voltages as voltage tune input which generates a continuous sweep from low to high frequency. This type of sweep is known as chirp signal. The transmitted signal is propagated to the target object from radar focused using horn antenna. The transmitted signal is reflected and propagated back to the receiver. We assume that the transmitter and receiver are co-located and synchronized. So the signal received by the radar is the replica of transmitted signal with a round trip propagation delay  $\Delta t$  to the target object. We can express the received signal during a chirp as follows,

$$x_r(t) = \sigma \cos[A(t) + \Phi(t)], \quad (8)$$

where  $A(t)$  and  $\Phi(t)$  can be expressed as,

$$A(t) = 2\pi f_0 t + \frac{\pi(f_1 - f_2)}{T} t^2, \quad (9)$$

$$\Phi(t) = -2\pi\Delta t f_0 + \frac{\pi(f_1 - f_0)}{T} (\Delta t)^2 - \frac{2\pi(f_1 - f_0)}{T} (\Delta t)t. \quad (10)$$

We have derived the in-phase ( $I$ ) output expression in Eq. (7). Eqs. (6) show how we can express the received signal as a summation of two terms. Using the same derivation procedure we can get the received signal as the summation of two terms in case of chirp signal pulses as,

$$F_{mix}(t) = \frac{\sigma}{2} \cos[2A(t) + \Phi(t)] + \frac{\sigma}{2} \cos\Phi(t). \quad (11)$$

Putting the values of  $A(t)$  and  $\Phi(t)$  from Eqs. (9) and (10) respectively, we get a new expression for Eq. (11). The former term in Eq. (11) is a chirp having minimum frequency  $4\pi f_0$  and the latter term is a cosine oscillation of frequency  $\frac{2\pi(f_1 - f_0)}{T} (\Delta t)t$ . As the transmitted pulse is narrowband that means  $f_0 \gg (f_1 - f_0)$ , we can discard the first term using a low-pass filter from signal represented by Eq. (11). The in-phase ( $I$ ) signal can be expressed only with the second term,  $I(t) = \frac{\sigma}{2} \cos\Phi(t)$ . Now we substitute the value of  $\Phi(t)$  from Eq. (10) in the above mentioned second term to obtain the relation between cosine signal and range of the target object. In Eq. (10) we discard terms containing  $f_0$  as it is large compared to the Doppler frequency and as we have used low-pass filter for getting the  $I$ -channel signal. Therefore, the  $I$ -channel signal can be expressed as,

$$I(t) = \frac{\sigma}{2} \cos\left[\frac{4\pi f_0 r_0}{c} + \frac{4\pi(f_1 - f_0)r}{cT} t\right]. \quad (12)$$

Similarly, we can get the  $Q$  output as,

$$Q(t) = -\frac{\sigma}{2} \sin\left[\frac{4\pi f_0 r_0}{c} + \frac{4\pi(f_1 - f_0)r}{cT} t\right]. \quad (13)$$

Finally, we discuss about computing range and velocity using multiple chirp pulses which in our case are ramp pulses. If we assume that the target is moving with a constant velocity and we express the motion as

$$r(\xi) = r_0 + \dot{r}\xi, \quad (14)$$

where  $r_0$  is the range of the object at time instant zero,  $\dot{r}$  is range-rate or velocity of the target object and  $\xi$  is called slow time. The time at which each successive pulse is transmitted from the radar is known as slow time and fast time is the typical time taken by the signal propagation. If we substitute the value of  $r$  from Eq. (14) into Eqs. (12) and (13), we get the following two new equations:

$$I(t, \xi) = \frac{\sigma}{2} \cos\left[\left(\frac{4\pi f_0}{c} + \frac{4\pi(f_1 - f_0)}{cT} t\right)(r_0 + \dot{r}\xi)\right], \quad (15)$$

and

$$Q(t, \xi) = -\frac{\sigma}{2} \sin\left[\left(\frac{4\pi f_0}{c} + \frac{4\pi(f_1 - f_0)}{cT} t\right)(r_0 + \dot{r}\xi)\right]. \quad (16)$$

If we sample  $I$  and  $Q$  we get functions of fast time  $t$  and slow time  $\xi$ . Therefore,  $I$  and  $Q$  are two-dimensional functions.  $I$  and  $Q$  vary in fast time  $t$  with frequency  $\frac{2r_0(f_1 - f_0)}{cT}$  which is proportional to the target range.  $I$  and  $Q$  also vary with the slow time with frequency  $\frac{2\dot{r}f_0}{c}$ , which is proportional to the target velocity or range-rate. Now we can perform a two-dimensional FFT on the analytical signal  $F(t, \xi) = I(t, \xi) + iQ(t, \xi)$  and scale the graph axes properly to get an ambiguity function that determines the target range and velocity correctly.

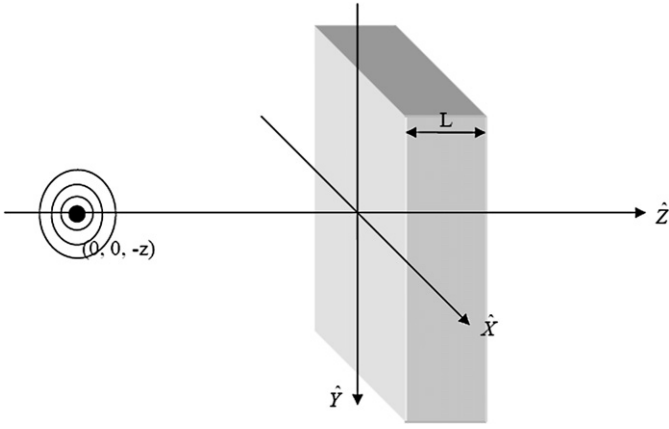


Fig. 3. Wave propagation from a point source through a medium (source [8]).

#### 2.4. Relation between material refractive index and reflectivity of microwave signal

We use a model developed for Through-the-Wall Imaging (TWI) in THz range [7,8]. The model offers the reflectivity of plain electromagnetic wave from different types of material surfaces in THz frequency range. Our proposed integrated radar mote includes a  $K_a$ -band Doppler radar. Therefore, we extend the existing reflectivity model to incorporate Doppler shift and relevant frequency band in our experimental radar. In this section we explain the existing model while our modified model will be discussed in later section.

For the existing model [7,8], we consider reflecting materials to be non-conducting for simplicity. Since the materials are assumed to be non-conducting, they have no conductivity and constant permittivity. Therefore, the refractive index is constant and real-valued for a specific material type. Reflectivity of a radar signal depends on some factors and material property is one of those important factors. The reflectivity model equation and transfer function of the reflecting medium are obtained from planar expansion of the Green's functions by employing spherical coordinates [8]. Consider that the wave propagates into the medium with an index of refraction ( $n_m$ ). The source of the signal is located at  $r_0 = -z_0\hat{z}$  and coordinates are shown in Fig. 3.

The wave equation with source  $s(r, t)$  is given as follows:

$$\nabla^2 E - \frac{n^2}{c^2} \frac{\partial^2 E}{\partial t^2} = s(r, t). \quad (17)$$

Here,  $E$  is the electric field intensity,  $n$  is the refractive index,  $c$  is the speed of light,  $s(r, t)$  is the source at time  $t$  and location  $r$ . Now we express the source terms of angular frequency ( $\omega$ ) as follows,

$$s(r, t) = \frac{1}{2\pi} \int_{-\infty}^{\infty} S(r, \omega) e^{i\omega t} d\omega. \quad (18)$$

Here,  $S(r, \omega)$  is the source angular frequency. Next we use the identity between angular frequency and oscillation frequency as follows  $\omega = 2\pi\nu$  and  $d\omega = 2\pi d\nu$ . Based on the solution of the plane wave equation, we get a time independent wave equation. Substituting the source at point  $r_0 = -z_0\hat{z}$  and using Green's function we get the following equation,

$$(\nabla^2 + k^2 n^2(z))g(r, r_0) = \delta(r + r_0) = \delta(x)\delta(y)\delta(z + z_0). \quad (19)$$

Here wave number is  $k = 2\pi/\lambda$  and  $\lambda$  is the wavelength in free space. The refractive index of the system is,

$$n(z) = \begin{cases} 1 & \text{for } z < 0, \\ n & \text{for } 0 \leq z \leq L, \\ 1 & \text{for } L < z. \end{cases} \quad (20)$$

From Fig. 3 we observe that the refractive index is 1 as the medium between the point source and the reflective object is air and that is shown in first condition of Eq. (20). Similarly  $n(z)$  is equal to the refractive index of the medium when the wave propagates inside the reflective object and finally the refractive index is 1 when the signal reaches in air passing through the medium. Some portion of the wave passes through the object and some portion is reflected back to the source. We are concerned about the reflected portion, so the first two conditions of Eq. (20) are relevant for our system. The frequency domain solution for  $E$  is given as,

$$E(r, \nu) = \int g(r, r_0) S(r, \nu) d^3 r_0 \quad (21)$$

where  $g(r, r_0)$  is the Green's function in the spatial domain. The time domain solution of  $E$  is computed doing the inverse Fourier transform of Eq. (21). Due to the assumption that the materials are non-conductive, the electromagnetic wave can propagate the medium with little damping [8]. As we have put the source at  $r_0 = -z_0\hat{z}$  along the  $\hat{z}$  direction, Eq. (19) can be converted in Fourier domain, and using the wave number definition we can get the homogeneous wave equation. The solution of the homogeneous wave equation can be expressed as a sum of two terms: right going wave or wave transmitted through the medium and left going wave or wave reflected back to the source. The solutions of the wave equations in each region must satisfy the boundary conditions, which state that the wave and derivative must be continuous at all boundaries. Then we can compute the coefficients of each component wave. If the refractive index obeys the three conditions mentioned in Eq. (20), we can get the solution for the coefficient of the Green's function. Using the solutions of the coefficient of the Green's function the reflection and transmission amplitudes can be expressed in terms of incident wave, reflected wave and wave transmitted through medium.

A few algebraic simplifications of Eq. (21) and solutions of the coefficient of the Green's function yield the reflectance or reflectivity coefficient

$$R = \frac{(N - N_m) + (N_m - N)e^{i2L\sqrt{N_m}}}{\sqrt{N_m} + \sqrt{N^2 - N_m} - \sqrt{N_m} - \sqrt{N^2 - N_m}e^{i2L\sqrt{N_m}}} \quad (22)$$

where,

$$\sqrt{N_m} = \sqrt{n_m^2 k^2 - (2\pi\nu_x)^2 - (2\pi\nu_y)^2}, \quad (23)$$

and

$$\sqrt{N} = \sqrt{k^2 - (2\pi\nu_x)^2 - (2\pi\nu_y)^2}. \quad (24)$$

Here,  $n_m$  is the refractive index of the reflecting material,  $L$  is the thickness of the reflecting material,  $k$  is the wave number and  $k = 2\pi f/c$ ,  $c$  is the speed of light,  $\nu_x = 1/\lambda_x$  and  $\nu_y = 1/\lambda_y$ , and  $\lambda$  is the wavelength of the electromagnetic signal.  $1/\lambda$  is known as wave number in electromagnetic radiation. Here  $\nu_x$  and  $\nu_y$  are  $x$ -axis and  $y$ -axis components of the wavenumber. Now using the spherical coordinate representation we obtain,  $2\pi\nu_x = k \sin\theta \cos\theta$ ,  $2\pi\nu_y = k \sin\theta \sin\theta$ , and  $2\pi\nu_z = k \cos\theta$  and putting these values in Eqs. (23) and (24) we get,

$$\sqrt{N_m} = k\sqrt{n_m^2 - \sin^2\theta}, \quad (25)$$

$$\sqrt{N} = k\sqrt{1 - \sin^2\theta} = k \cos\theta. \quad (26)$$

Now inserting the above results in Eq. (22) we obtain the reflectivity as follows [8],

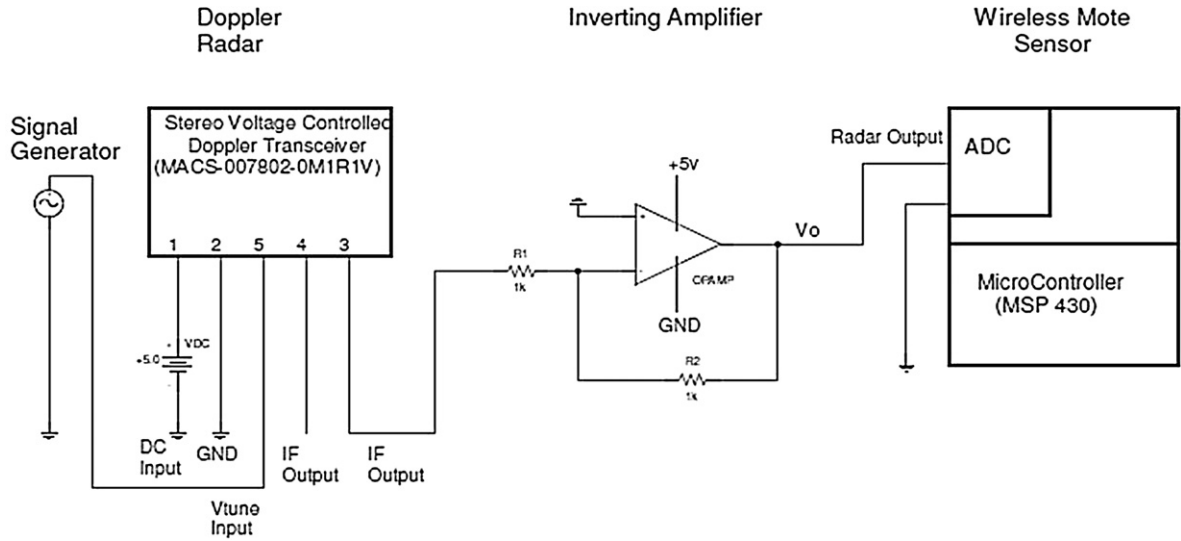


Fig. 4. Schematic diagram for integration of  $K_a$ -band Doppler radar and TelosB wireless sensor platform.

$$R(\theta) = \frac{(1 - n_m^2) + (n_m^2 - 1)e^{i2kL\sqrt{n_m^2 - \sin^2\theta}}}{(\sqrt{n_m^2 - \sin^2\theta} + \cos\theta)^2 - (\sqrt{n_m^2 - \sin^2\theta} - \cos\theta)^2 e^{i2kL\sqrt{n_m^2 - \sin^2\theta}}}. \quad (27)$$

If we consider the incident wave angle  $\theta = 0$ , then we obtain:

$$R = \frac{(1 - n_m^2) + (n_m^2 - 1)e^{i2kn_mL}}{(n_m + 1)^2 - (n_m - 1)^2 e^{i2kn_mL}}. \quad (28)$$

### 3. Design and methods

In this section we start describing the design and implementation of our proposed integrated radar–mote sensor system. Next, a modified version of the reflectivity model is proposed.

#### 3.1. Design and implementation of integrated sensor systems

This section describes our integrated sensor system. Commercially available wireless sensor mote platforms are often equipped with a range of built-in passive sensors such as light, temperature, vibration etc. Standard mote platforms also support the extension of sensor modalities by allowing specific plug-in sensor circuit boards using the standard expansion ports of the mote. For example, WiEye and SBT80 built by EasySen are two standard sensor circuit boards which can work with TelosB through its expansion ports [18]. Our miniature Doppler radar has an output pin that produces analog output signal. We connect the output pin of the miniature Doppler radar to the analog expansion input pin of TelosB in our integrated autonomous sensor suite. Using the built-in analog-to-digital converter (ADC) in the microcontroller (MSP430) of TelosB mote, we sample the analog radar output. We modify the user program to allow the sampling of the analog signal at different rates using adjustable program parameters.

The ADC core converts the analog input to a 12 bit digital representation and stores the results in conversion memory. We can use two reference voltage levels  $V_{R+}$  (maximum) and  $V_{R-}$  (minimum), which are selectable by programming. The formula of converting analog signals to digital is represented in the following equation,

$$N_{ADC} = 4096 * \frac{V_{in} - V_{R-}}{V_{R+} - V_{R-}}. \quad (29)$$

The first step is the hardware level integration of the Doppler radar and wireless mote. Fig. 4 shows the schematic diagram of the integrated radar–mote sensor system.

The next step is the software-level integration. We replace the data capturing task from manual processing to autonomous recording at the TelosB mote using hardware level design. This step requires connecting analog radar output as analog input of the already available ADC of the TelosB and sampling the analog signal using the ADC12 with the help of a user program stored in the mote. We have a base station TelosB mote connected to a workstation via USB port. A user program is loaded into the base station mote to manage the wireless connection between the sensing mote and the workstation. We can trigger the sensing mote with an ACTIVATE signal from the workstation to the sensing mote via base station.

Our user program defines and configures the components and modules required for the desired operation of digitizing an analog signal and sending it to a base station wireless mote. The digitized data is stored in internal flash buffer. The wireless control module sends the data as small packets. The host computer through the base station mote can store the sensed data from a remote radar sensor mote.

#### 3.2. Reflectivity model of microwave signals adopted to incorporate Doppler shifts

The reflectivity model discussed in an earlier section describes the reflectivity of plane wave from different types of non-conducting surface [7,8]. This section discusses our modifications to the plane wave reflectivity model to incorporate Doppler principle. Adding Doppler shift to the plane wave does not change the amplitude of the original signal. The plane wave model in Eq. (28) can be re-written using Doppler shift as follows [8],

$$R = \frac{(1 - n_m^2) + (n_m^2 - 1)e^{i\omega n_m L}}{(n_m + 1)^2 - (n_m - 1)^2 e^{i\omega n_m L}}. \quad (30)$$

Here,  $\omega = 4\pi f/c$ ,  $c$  is the speed of light,  $f$  is the frequency of the plane wave signal,  $n_m$  is the refractive index of the reflecting material and  $L$  is the thickness of the reflecting material. The two outputs of the radar ( $Q$  and  $I$ ) can be expressed as,

$$F(t) = I(t) + iQ(t). \quad (31)$$

The  $I$ -channel radar output can be expressed as follows,

$$I = \frac{\sigma}{2} \cos[4\pi f_0 r/c], \quad (32)$$

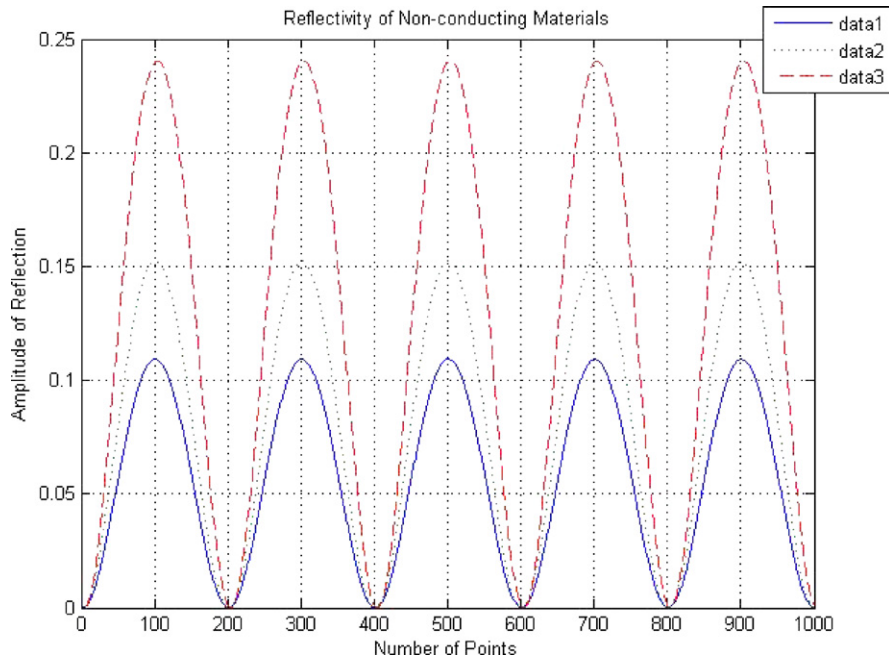


Fig. 5. Reflected Doppler radar signal from non-conducting materials.

where  $f_0$  is the carrier frequency,  $\sigma$  is a constant which corresponds to the target radar cross section (RCS) and  $r(t) = r_0 + \dot{r}t$ . Note  $r_0$  is a range at instant zero and  $\dot{r}$  is the rate at which the object is changing its range, range-rate or velocity of the object. The  $Q$ -channel signal or  $Q(t)$  can be expressed similarly as,

$$Q = \frac{\sigma}{2} \sin[4\pi f_0 r/c]. \quad (33)$$

Substituting Eqs. (32) and (33) into Eq. (31) and using well-known identity,  $e^{ix} = \cos x + i\sin x$ , we can write  $F(t)$  as,

$$F(t) = \frac{\sigma}{2} e^{\frac{i4\pi f_0 r}{c}}, \quad (34)$$

and finally,

$$F(t) = \frac{\sigma}{2} e^{i\omega r}. \quad (35)$$

Now we are ready to derive an approximation for the reflectivity index to include the Doppler shift. Based on Eqs. (30), (34), (35), and ignoring the Doppler effect within the non-conducting material, we arrive at the following expression for the reflectivity,

$$R = \frac{(1 - n_m^2) + (n_m^2 - 1)e^{i[4\frac{\pi}{c}(f_0 r_0 + f_0 nL + (f_1 - f_0)/T\dot{r}t) ]}}{(n_m + 1)^2 - (n_m - 1)^2 e^{i[4\frac{\pi}{c}(f_0 r_0 + f_0 nL + (f_1 - f_0)/T\dot{r}t) ]}}. \quad (36)$$

Eq. (36) is our final approximate reflectivity model of different non-conducting materials considering Doppler effect between radar and the material.

#### 4. Experimental results

In this section we describe the experimental results of the reflectivity of non-conducting materials based on the modified reflectivity model. We design experiments to test the capability of the newly built system and to validate the result of the simulations. We process the data with simple signal processing techniques to compute the range velocity of the targets. We classify different types of non-conducting materials exploiting extracted features from the Doppler data.

##### 4.1. Simulation results on reflectivity for selected non-conducting materials

The reflective model derived in Eq. (36) assumes the reflective materials are non-conducting and homogeneous. Accordingly, we choose several non-conducting materials for reflectivity simulation. The example materials in our simulation are wood, paper and glass. The refractive indices of the materials depend on the frequency with which it is measured [8]. However, constraining the frequency range, the refractive index is constant with good accuracy for any material. For simplicity, we vary the index of refraction for the three materials in our experiment while keeping the frequency range the same as in our Doppler radar. Therefore, the simulated signal will represent the reflectivity of Doppler signals from those material surfaces. Typical refractive indexes of wood, commonly used glass and paper are 1.41, 1.51, and 1.73, respectively [7,8]. Fig. 6 shows the simulated reflectivity of Doppler radar signal using Eq. (36) for wood, glass, and paper, respectively. We show five pulses of the reflected signal for each case. The y-axis shows the amplitude of reflection and the x-axis indicates the number of data points per signal pulse (time). Fig. 5 confirms that our reflectivity model correctly obtains increased reflectivity for objects with higher refractive indices. The amplitude of reflection increases with the increase of the refractive index of the non-conducting materials, assuming that all other factors are constant or vary insignificantly.

Since we add the Doppler shift to our reflectivity model, the simulated signal shows the range and velocity of the target material along with reflectivity. Fig. 6 shows the plots of velocity vs. range of the simulated signal for wood reflector as an example. Note that the Doppler shift is not related to the amplitude of the reflected signal. Hence, we obtain the same plot for all three materials in our experiment. We perform Fast Fourier Transforms (FFT) of the simulated signal and obtain corresponding range and velocity plot. The distance between the moving target and the source of the signal is 0.5 m and 1 m as shown in Figs. 6(a) and 6(b) respectively and the corresponding velocity of the moving reflector is 0.5 m/s and 1 m/s for respective cases. Since the Doppler shift expression is the same for all the reflectors, we show the corresponding plots for one example reflector (wood) in this example.

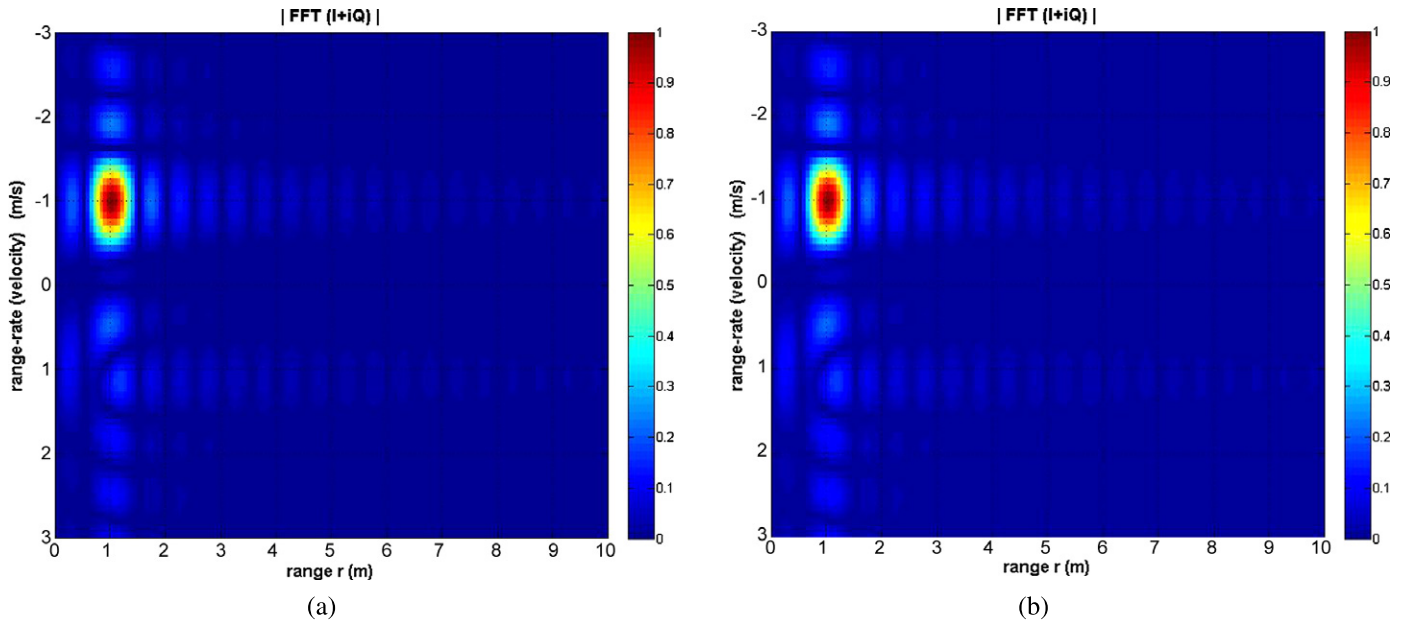


Fig. 6. Range-rate (velocity) vs. range plot of simulated signal, (a) the velocity of the target ( $\dot{r}$ ) was 0.5 m/s and distance ( $r_0$ ) between the reflector (wood) and the source of signal was 0.5 m, (b)  $\dot{r} = 1$  m/s and  $r_0 = 1$  m.

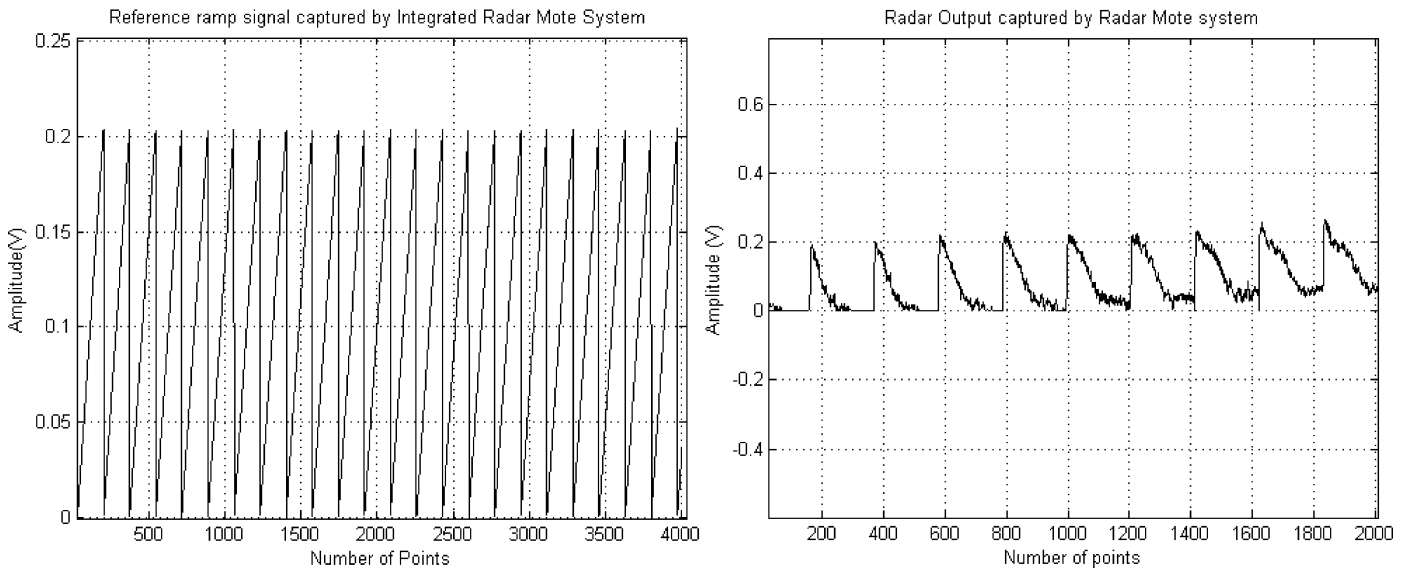


Fig. 7. (a) Ramp signal (peak to peak voltage 200 mV) captured and reconstructed using integrated wireless mote with sampling frequency of 200 KHz, (b) an example radar signal captured and reconstructed successfully by the integrated radar–mote system.

4.2. Testing the integrated radar mote sensor with sample data collection

In this section we present the test data collection using our integrated radar–mote system. We perform a series of baseline experiments with the initial integrated system and collect some known standard signals such as a ramp wave with certain amplitude and frequency. Fig. 7(a) shows a ramp wave captured and reconstructed by the integrated radar–mote system. We generate an analog signal with voltage output similar to the Doppler radar using the standard lab signal generator. The signal generator output is connected to the mote as ADC input instead of the radar output in this particular case. We captured the same ramp wave signal with a storage oscilloscope which was previously used to capture radar output. Comparing the ramp signal

captured with radar mote with that of the storage oscilloscope, we find that radar mote can capture the analog ramp signal with almost the same accuracy and precision as storage oscilloscope.

Finally, we test our integrated radar–mote system to collect radar output by connecting the radar output to the wireless mote. The stored data contains sampled digital value of the analog radar signal. Fig. 7(b) shows an example radar signal captured and reconstructed successfully by the integrated radar–mote system with significant accuracy. The reconstructed radar signal is slightly distorted as shown in Fig. 7(b). The observed slight distortions may be due to the unshielded amplifier circuit and connecting wires used to bridge the radar and sensor mote. However, this slight distortion does not have any significant impact on further processing as shown in subsequent results.

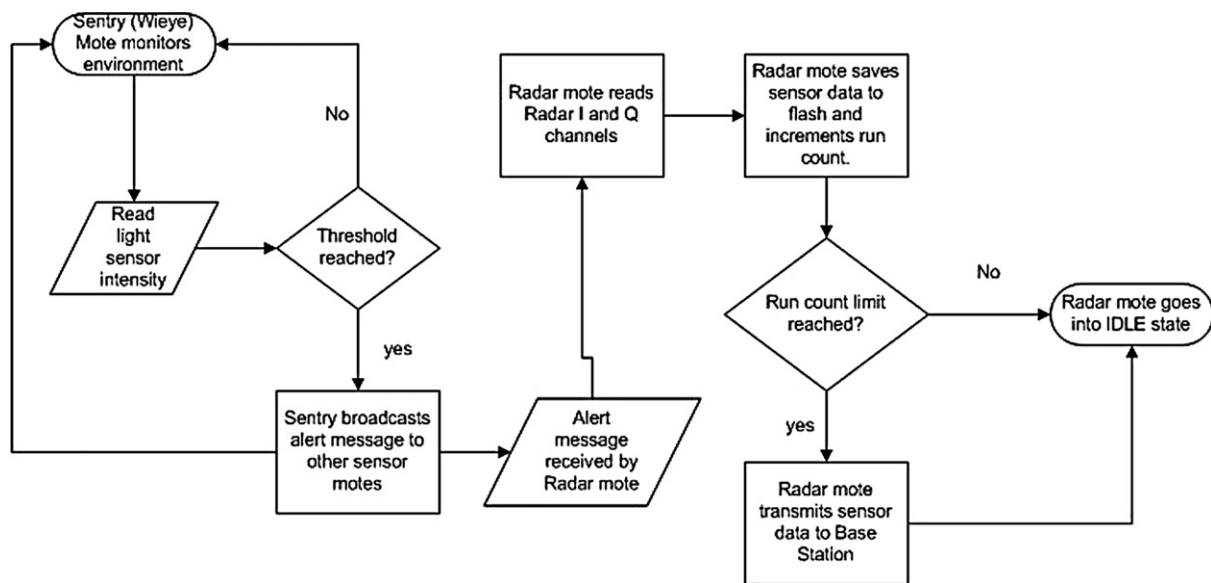


Fig. 8. Flow diagram showing the experiment process.

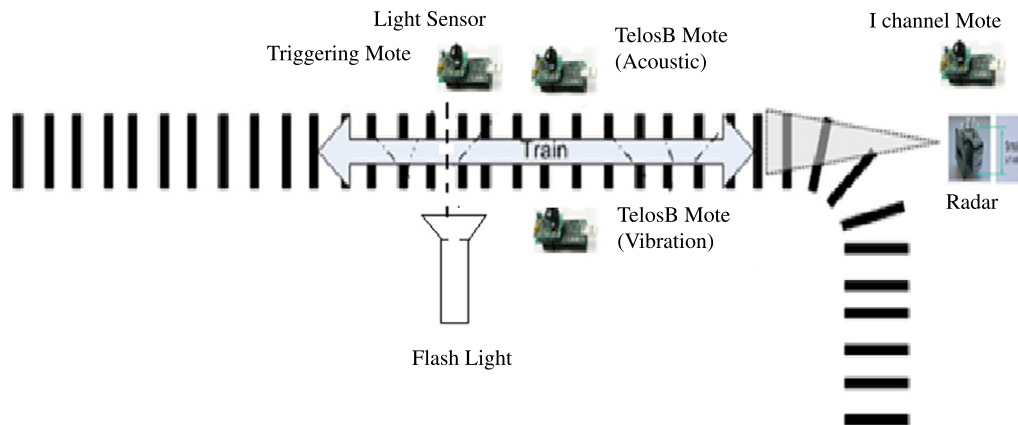


Fig. 9. The experimental setup of our autonomous distributed sensor including radar mote and SBT80 sensor motes [18].

#### 4.3. Experimental setup and data collection

In this section we discuss the experimental setup and different experimental scenarios using our integrated radar–mote system. The goal of the experiment is to explore the capability of the integrated radar–mote sensor system and validate the simulation observation about reflectivity of non-conducting materials. We use a toy train with different reflective materials mounted on it as our target. The train is run by battery power and moves round an oval shaped track. We emulate different events by making changes to the toy train configurations. Fig. 8 shows an overview of how the radar–mote system works during experiments and Fig. 9 shows the experimental sensor network setup with a toy train on the track.

We integrated SBT80 sensor board [18] with TelosB motes and use the visual light sensor on SBT80 to detect presence of a moving target and activate the radar–mote system to collect the data. Details of the experiments and results of velocity measurements and target classification are given in [10,11]. In the present work we focus on describing the results concerning material composition identification.

We use the raw radar signals for classifying the different materials the reflector is made of with the help of simple signal processing and classification algorithm. For testing, we create three different types of reflection profiles with three non-conducting materials such as wood, glass and paper (same materials used in

simulation) of the train. We place these different reflection materials at the front of the train such that the directed beam of radar signal is reflected back from these reflection plates. The data is collected for the same configuration with different speeds of the toy train and different distances between the radar mote and toy train. Table 2 summarizes different test cases for our toy train application.

##### 4.3.1. Experimental results on reflectivity for selected non-conducting materials

The simulated signal reflected from three non-conducting materials is discussed in Section 4.1. In this section, we collect the corresponding experimental radar signal reflected back from rectangular reflective plate made of the same non-conducting materials respectively. Figs. 10(a), (b) and (c) show experimental signals reflected back from reflector made of wood, glass, and paper respectively. The experimental signals in Figs. 10(a), (b) and (c) do not match exactly to the simulated signals in Fig. 5 in respect to magnitude values. However, they follow the same pattern of increase in reflection magnitude with increase of refractive indices of the non-conducting materials. Since the simulated model is a simplified case of reflectivity computation, the difference between simulation and experiment is expected. Furthermore, the reflectivity signal may be modulated by line frequency and hence the saw-tooth type pattern is visible in Fig. 10. The overall results

**Table 2**  
Different test configuration for toy train experiment.

| Configuration  | Type                | Description   |
|--|---------------------|---|
| Reflector  | Wood, glass, paper  | The front of the train holds a rectangular plate that works as a reflector. The reflector is made of the non-conducting materials (wood, glass, paper) in different configurations. |
| Range  | 0.8 m, 1.2 m, 1.6 m | The distance between the moving target and the static radar is 0.8 m, 1.2 m, 1.6 m for two different configurations.  |
| Velocity (position of speed control dial of the toy train) | 100, 80, 60         | The toy train has a dial to control the speed of the train. The value in previous column indicates the position of the dial such as 100, 80, 60.                                    |

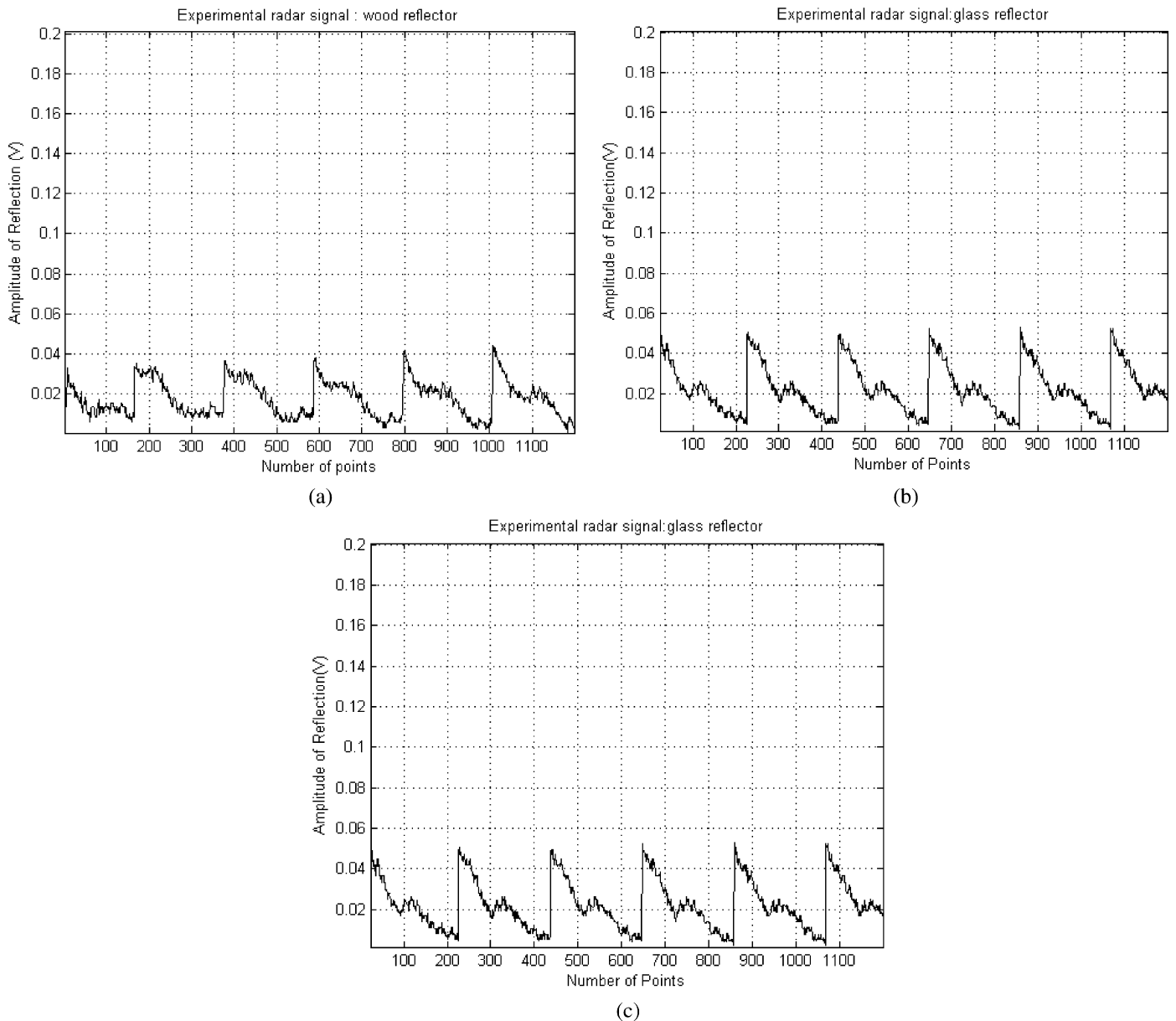


**Fig. 10.** Experimental signal reflected back from (a) wood reflector, (b) glass reflector and (c) paper reflector.

show that the reflectivity of the materials is an important factor which influences how much energy reflects back to source from a materials surface.

#### 4.3.2. Experimental results on reflectivity for selected non-conducting materials

One of the goals of this work is to explore whether we can use material properties, specifically refractive index of materials, to classify the materials types of the targets. For simplicity and

limited scope of this work, we obtain a modified model for non-conducting materials as shown in Eq. (36). We collect reflected radar signals from three non-conducting materials such as wood, glass and paper with our integrated radar-mote autonomous system. The pseudo-spectrum of the signal, computed with MUSIC algorithm, is selected as the feature to classify the non-conducting material types of the target. The MUSIC technique has been widely used in telecommunication, biomedical, signal processing and electromagnetic disciplines to solve problems such as spectrum and

**Table 3**  
Result of classification with WEKA machine learning tool.

| Class              | Number of runs | Classifier   | True positive rate | False positive rate | ROC area | Kappa statistic | Accuracy (%) |
|--------------------|----------------|--|--------------------|---------------------|----------|-----------------|--------------|
| Wood, glass, paper | 540            | Random Forest  | 0.74               | 0.13                | 0.89     | 0.60            | 73.82        |
|                    |                | LMT: Logistic Model Trees (Decision tree based)              | 0.77               | 0.12                | 0.90     | 0.66            | 77.04        |
|                    |                | Functional Tree (Decision tree based on logistic regression) | 0.77               | 0.12                | 0.84     | 0.65            | 76.67        |
|                    |                | Support Vector Machine (SVM)                                 | 0.76               | 0.12                | 0.82     | 0.63            | 75.56        |
|                    |                | Multilayer Perceptron  | 0.80               | 0.10                | 0.92     | 0.70            | 79.81        |

signal estimation, the direction of arrival [19–23]. The MUSIC algorithm estimates the pseudo-spectrum of a signal using Schmidt's eigenspace analysis method [24]. The MUSIC algorithm produces a spectral estimate of a signal performing the eigenvector–eigenvalue decomposition of the autocorrelation matrix of the signal [25].

We provide a brief description of the classification process here. Each instance of the radar signal is treated as one run and we collect 20 instances for all three non-conducting reflecting materials for each configuration. We take the raw signal for each instance and perform preprocessing. The MUSIC technique is then applied to the signal to obtain feature vector for that instance following the steps shown in Fig. 11. Then we classify the instances with WEKA machine learning toolbox with some standard classifiers available in WEKA. Table 3 shows the result of classification using different types of classifier for the three non-conducting materials.

The classifiers used from WEKA toolbox are random forest, logistic model tree (LMT), functional tree, Multilayer Perceptron (MLP) and support vector machine (SVM). Table 3 shows that Multilayer Perceptron classifier provides the highest percentage of accuracy when individually compared to the other classifiers. The classifier accuracy is between 75–80% for most of the classifiers which is reasonably good considering the very small variations in classes. The area under ROC overall, which is another test of accuracy, is also in the range of 0.8 to 0.9 in scale of 1.0 for most of the cases. The Kappa statistic is a measure of the stability for machine learning applications. If the Kappa statistic value is greater than 0.6, it indicates substantial agreement for the classification result [26]. For most of the classifiers in Table 3 the Kappa statistic is above 0.6. Therefore, the classification results are substantially stable.

#### 4.4. Comparison of our integrated radar–mote system to standalone systems

The aim of our work is to integrate a powerful active sensor such as Doppler radar into a wireless sensor mote, which achieves all the capabilities of the standalone radar systems. Table 4 shows a summary comparison between an integrated radar–mote system versus standalone radar system.

#### 4.5. Comparison of our integrated radar–mote system with other similar systems and potential applications

Integrated radar–mote system is emerging as an effective technology for detection, classification, surveillance and tracking applications [2,10,11,13,27]. Recently the Samraksh Company launched a new product which is a modification of BumbleBee known as GuardBee [28]. GuardBee integrates BumbleBee pulsed Doppler Radar (PDR) with an ultra-low power FPGA board which eliminates the need of an additional wireless mote previously used for signal processing. The Pulsed Doppler radar used in BumbleBee has a center frequency of 5.8 GHz [13]. Furthermore, although BumbleBee has the capability to compute range, velocity and direction of moving target, computation of range involves complex off line signal post processing [13].

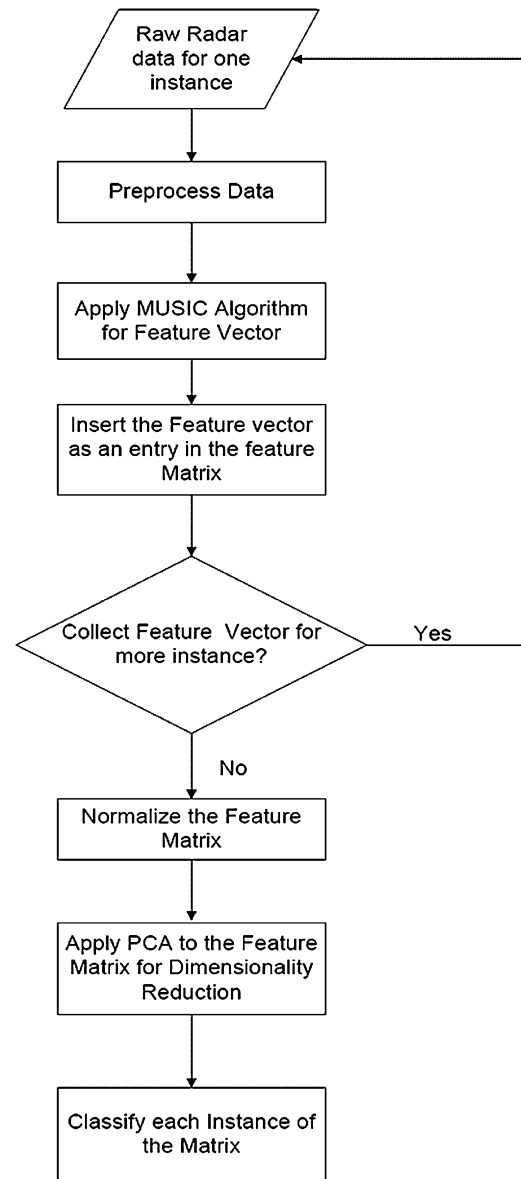


**Fig. 11.** Methods of feature extraction and classification.

Our prototype integrated radar sensor mote, on the other hand, is implemented using low-cost commercial-off-the-shelf components [10]. We use a K-band Doppler radar with a center frequency of 24.125 GHz with electronic tuning system capable of varying the frequency within a bandwidth of 0.3 GHz. Therefore, our system is amenable to applications operating in higher frequency band such as in K-band. Our prototype system has a capability to compute the range, velocity and direction of moving target by simply applying Fast Fourier Transform to captured raw data with very little preprocessing.

**Table 4**

Comparison between standalone radar and integrated radar–mote system.

| Features                    | Standalone Doppler radar                                  | Integrated radar–mote system | Description  |
|-----------------------------|---|------------------------------|--|
| Automated data collection   | No  | Yes                          | The standalone radar system usually needs human intervention to store data in the storage system. Some current digital oscilloscopes may have the software control over the data gathering. However, triggering the digital scope requires complex circuitry and system to operate. Whereas in the integrated radar–mote system data gathering system is automated with the help of the wireless network framework of the wireless motes.  |
| Event driven                | No  | Yes                          | The data capturing is triggered when the integrated radar mote gets a triggering signal from a sentry node. In our case the WiEye sensor mote sends the triggering signal when it detects the presence of any object within its field of view. Similar ways using the other sensors available in the wireless node different triggering events can be designed. Whereas the data capturing is not event driven in case of the standalone radar system.   |
| Large-scale data collection | Not suitable  | Suitable                     | In case of the standalone system requires human intervention and the storage oscilloscope also takes at least 5 seconds to store the data at any instant. Therefore, the standalone system is not suitable for large scale data collection where one needs to collect many instances of a repeatable event.  |
| Portability and mobility    | Not easily portable and not suitable for remote operation | Yes                          | Need large supporting systems like oscilloscope, signal generator and power supply. Therefore, the standalone system cannot be deployed at any place due to specific requirements of the supporting equipments. Whereas the storage oscilloscope is replaced with the tiny wireless mote in the integrated system and the motes are run by battery power. The work is going on to replace the signal generator and power source equipments with the on-board signal generator and power source circuit. That would make the integrated system fully portable and mobile. |
| Remote operation            | Not suitable  | Suitable                     | The integrated system can be triggered by the sentry nodes from a distant place through wireless communication. Similarly the base station node which works as bridge between the integrated system and a workstation can also be placed in distant place from the integrated radar mote.  |
| Power requirement           | High  | Low                          | The wireless mote which replaces the storage oscilloscope is run by 3 battery power. Whereas the scope requires high power source to operate   |

In addition, fusion of PDR passive infrared (PIR) sensor enables our system to automatically trigger when a moving object enters in the field of view. Consequently, the data collection process is fully autonomous that makes our system suitable to use in real life repeatable experiments without any human intervention. The sample experiments in this work demonstrate that this radar–mote system can be used for effective surveillance and tracking of moving objects (human, animal, or vehicles) as well as non-cooperative target similar to comparable wireless radar sensor networks reported in the literature [27,29,30]. However, unlike similar systems [2,12,13,27,29], our prototype system offers additional capability of discerning target materials as demonstrated in this work. This capability may offer additional insights about target types in hostile environment.

## 5. Conclusion and future work

Our contribution in this work can be divided into two parts. The first contribution is a successful design and implementation of an integrated autonomous radar–mote system. The second contribution involves experimentation and simulation of reflectivity of non-conducting materials. We have modified an analytical reflectivity model [7,8] to incorporate Doppler shift. We obtain simulated Doppler signal for various non-conducting materials. Finally, we experimentally verify and classify the non-conducting material targets using real data collected with our newly designed radar–mote system.

We incorporate active radar sensor into the wireless sensor network. We successfully design and implement an autonomous radar–mote system integrating a  $K_a$ -band Doppler radar to TelosB wireless mote. Our integrated radar–mote system can successfully replicate the data collection capabilities of a standalone radar system. We experimentally collect reflected radar signals from the same three non-conducting materials using our newly implemented integrated radar–mote system. The radar–mote au-

tonomously captures large amounts of signal for different configurations. Our experimental radar–mote reflection data validates our simulated data for the selected non-conducting materials. Finally, we successfully classify three non-conducting materials using the collected reflectivity signals. The additional benefits of our integrated radar–mote system include increased automation, large-scale data collection, portability, remote operation and reduced power requirement.

The second part of the work proposes a modified reflectivity model [7,8] to obtain reflected signals from non-conducting material surfaces. The original model offers the reflectivity of a plane electromagnetic wave from non-conducting materials. We modify the model to incorporate Doppler shift into the reflectivity model such that the signal offers range-velocity information of the target in addition to reflectivity of different target materials. We simulate reflectivity of three non-conducting materials such as wood, glass and paper using our modified reflectivity model. The simulated signal is processed with FFT to compute range and velocity from Doppler shift. The simulation results confirm that the Doppler shift is successfully incorporated into the analytical reflectivity model.

In this work, we assume Doppler effect is negligible while signal travels within the non-conducting material for simplicity. In future, more accurate derivation for reflection and Doppler effects inside the material needs to be considered. This will allow one to study material specific reflection and its interaction with Doppler property within a material in addition to free space Doppler phenomena studied in this work. Furthermore, there is still opportunity to improve the system. The heavy laboratory equipments used in current setup pose inconveniences such as lack of portability and mobility. In a new generation of radar–mote integration, we replaced the standard laboratory signal generator and power supply equipment with equivalent on-board circuit implementation [31]. Such design is expected to be less affected by line frequency as noted in this work. Implementing the whole exper-

imental radar–mote system in a single IC package would be the final target. This work can be extended to explore object detection for different types of conducting as well as non-conducting materials in complex outdoor environment. One of the directions of improvement is to integrate the reflectivity of the conducting materials into our model. Successful integration of conducting materials into the model will make the model complete and applicable for a range of practically relevant scenarios.

## Acknowledgments

Part of this work is funded by FedEx Institute of Technology under Center for Large-Scale Integrated Optimization & Networks (CLION). Technical and equipment support is provided by Sensors Directorate, US Air Force Research Laboratory and Department of Electrical & Computer Engineering, University of Memphis.

## References

- [1] J. Hill, R. Szewczyk, A. Woo, S. Hollar, D. Culler, K. Pister, System architecture directions for networked sensors, *SIGPLAN Not.* 35 (11) (November 2000) 93–104.
- [2] P. Dutta, A. Arora, S. Bibyk, Towards radar-enabled sensor networks, in: *ISPN'06*, Nashville, Tennessee, USA, April 19–21, 2006.
- [3] J. Yick, B. Mukherjee, D. Ghosal, Wireless sensor network survey, *Comput. Netw.* 52 (12) (August 2008) 2292–2330.
- [4] W. Dargie, C. Poellabauer, *Fundamentals of Wireless Sensor Networks: Theory and Practice*, John Wiley and Sons, 2010.
- [5] K. Sohraby, D. Minoli, T. Znati, *Wireless Sensor Networks: Technology, Protocols, and Applications*, John Wiley and Sons, 2007.
- [6] Mark A. Richards, *Fundamentals of Radar Signal Processing*, McGraw–Hill, 2005.
- [7] J. Kim, Through-the-wall imaging from electromagnetic scattered field measurements, A thesis for partial fulfillment of MS in Physics from Naval Post Graduate School, March 2007.
- [8] K. Lee, THz-imaging through-the-wall using the Born and Rytov approximations, A thesis for partial fulfillment of MS in Physics from Naval Post Graduate School, December 2008.
- [9] T. McEwen, Ultra-wideband radar motion sensor, Pat. #5361070.
- [10] R. Kozma, L. Wang, K. Iftekharuddin, E. McCracken, M. Khan, K. Islam, R.M. Demirel, Multi-modal sensor system integrating COTS technology for surveillance and tracking, in: *Proceedings of IEEE Radar 2010 Conference*, Washington, DC, USA, 10–14 May 2010, pp. 1030–1035.
- [11] R. Kozma, L. Wang, K. Iftekharuddin, E. McCracken, M. Khan, K. Islam, S. Bhurtel, R.M. Demirel, Radar-enabled collaborative sensor network integrating COTS technology for surveillance and tracking, *Sensors* 12 (2012) 1136–1151.
- [12] TWR-ISM-002-I Radar: Hardware User's Manual, Advantaca Inc., 2002.
- [13] Users manual for the BumbleBee (Model 0): A mote-scale pulsed Doppler radar for use in wireless sensor networks, The Samraksh Company.
- [14] Obtained: TelosB datasheet, [http://www.xbow.com/Products/Product\\_pdf\\_files/Wireless\\_pdf/TelosB\\_Datasheet.pdf](http://www.xbow.com/Products/Product_pdf_files/Wireless_pdf/TelosB_Datasheet.pdf).
- [15] Stereo voltage controlled Doppler transceiver datasheet, Obtained from: <http://www.macomtech.com/datasheets/MACS-007802-0M1R1V.pdf>.
- [16] R. Deming, Determining target range and velocity using Doppler radar, in: *FIT-AF Workshop*, FIT, University of Memphis, January 2009.
- [17] L. Shen, J. Kong, *Applied Electromagnetism*, second edition, PWS Publishers, Boston, MA, 1987.
- [18] SBT80 Datasheet, Obtained from: <http://www.easysen.com/support/SBT80v2/DatasheetSBT80v2.pdf>.
- [19] P. Stoica, R. Moses, *Introduction to Spectral Analysis*, Prentice Hall, Englewood Cliffs, NJ, 1997.
- [20] T. Georgio, Signal estimation via selective harmonic amplification: MUSIC, *IEEE Trans. Acoust. Speech Signal Process.* 48 (3) (2000) 780–790.
- [21] Z. Tian, Iterative MUSIC: coherent signal estimation, performance analysis, in: *IEEE Int. Conf. Acoustics, Speech and Signal Processing*, May 2002, pp. 3041–3044.
- [22] Y. Wei, F. Zenghe, A new method for joint DOA and FOA estimation using MUSIC algorithm, in: *Fourth Int. Conf. Microwave and Millimeter Wave Technology*, August 2004, pp. 219–222.
- [23] M. Secmen, G. Turhan-Sayan, Radar target classification method with reduced aspect dependency and improved noise performance using multiple signal classification algorithm, *IET Radar Sonar Navig.* 3 (2009) 583–595.
- [24] S. Marple, *Digital Spectral Analysis*, Prentice Hall, Englewood Cliffs, NJ, 1987, pp. 373–378.
- [25] R. Schmidt, Multiple emitter location and signal parameter estimation, *IEEE Trans. Antennas and Propagation AP-34* (March 1986) 276–280.
- [26] A. Viera, J. Garrett, Understanding interobserver agreement: The Kappa statistic, *Fam. Med.* 37 (5) (2005) 360–363.
- [27] M. Arik, O.B. Akan, Collaborative mobile target imaging in UWB wireless radar sensor networks, *IEEE J. Sel. Areas Commun.* 28 (6) (August 2010).
- [28] Users manual for the GuardBee: An ultra low-power, FPGA-based motion detection module, The Samraksh Company.
- [29] Y. Kim, A. Vu, J. Han, Tracking a moving target in wireless sensor networks using PDR sensors, in: *Proceedings of International Conference on Information Networking (ICOIN)*, January 26–28, 2011, Barcelona, pp. 394–398.
- [30] J. Lim, I. Wang, A. Terzis, Tracking a non-cooperative mobile target using low-power pulsed Doppler radars, in: *Proceedings of IEEE 35th Conference on Local Computer Networks (LCN)*, October 10–14, 2010, pp. 913–920.
- [31] R. Kozma, T. Tanigawa, O. Furrhi, S. Consul, Autonomous decision support in heterogeneous sensor networks, in: *Proc. SPIE 2012*, Baltimore, April 23–27, 2012.

**Muhammad M. Khan** is a PhD student at University of Memphis. He received his MS in Electrical & Computer Engineering from University of Memphis in 2010. He completed his BS in Computer Science & Engineering from Jahangirnagar University in 2006. His research interest includes intelligent systems, data mining and machine learning.

**Dr. Khan M. Iftekharuddin** is a professor in the department of electrical and computer engineering, a member of biomedical engineering program at Old Dominion University (ODU) and the director of ODU Vision Lab. Prior to ODU he was an associate professor in the department of electrical and computer engineering, biomedical engineering and bioinformatics program at the University of Memphis (UoM). He was an assistant professor of computer science and electrical and computer engineering at North Dakota State University (NDSU) before joining to the UoM. He is the principal author of one book and more than 150 journal papers, conference proceedings, and multiple book chapters. He serves as an Associate Editor for *Optical Engineering*, *International Journal of Image Processing* and *International Journal of Tomography and Statistics* and is on the editorial board of the journal *Computer Methods in Biomechanics and Biomedical Engineering: Imaging & Visualization*. He is a Fellow of the SPIE, a Senior Member of the IEEE, and a member of the OSA.

**Ernest McCracken** graduated with a Master's in Computer Science from the University of Memphis. His academic research focused on Wireless Sensor Networks (WSN) and Internet Metrics and Monitoring. His work included integration of micro radars on WSN motes and the NetViews project which monitored inter-domain network paths on the Internet in real time. He currently works as an Enterprise Development Lead for FedEx Services automation systems.

**Khandakar M. Islam** is working as Business and Integration Analyst II at Business & Finance Support Services, The University of Memphis. He is affiliated with CLION – Center for Large-Scale Integration and Optimization Networks and also working for his Master Thesis in Electrical and Computer Engineering, The University of Memphis. His research interest includes localization & tracking in Wireless Sensor Networks and Data Mining.

**Sushil R. Bhurtel** joined the University of Memphis in the fall 2009 as a graduate research assistant. Before joining the university he worked as a full time lecturer for nearly four years at Khwopa Engineering College, Kathmandu, Nepal. He received his Bachelors in Computer Engineering from Pokhara University in 2005 and is a life-time member of Nepal Engineering Council. His primary research interest is radar object recognition. He graduated from the University of Memphis in December 2011.

**Dr. Lan Wang** is an associate professor in the Computer Science Department at the University of Memphis. She holds a BS degree (1997) in Computer Science from Peking University, China and a PhD degree (2004) in Computer Science from University of California, Los Angeles. Dr. Wang's research interests include Internet architecture, Internet routing, network security, network performance measurement and sensor networks.

**Dr. Robert Kozma** is First Tennessee University Professor, Director of the Center of Large-Scale Integration and Optimization Networks (CLION), The University of Memphis, TN, USA. He holds a PhD in Physics (Delft,

Netherlands), MSc in Mathematics (Budapest, Hungary), MSc in Power Engineering (Moscow, Russia). Dr. Kozma has over 30 years of research experience in the design, analysis, and control of intelligent systems. Previous appointments include Associate Professor at Tohoku University, Sendai, Japan, and Lecturer at Otago University, New Zealand. He held visiting

positions with UC Berkeley, NASA/JPL Robotics, Sarnoff Co., Princeton, NJ, AFRL Hanscom AFB, MA. He has been General Chair of IJCNN2009, serves on IEEE CIS AdCom, INNS Board of Governors. Dr. Kozma has published 7 books and about 200 articles in international journals and conference proceedings.